3rd Solar Orbiter Workshop Sorrento, 25-29 May 2009

HYDRODYNAMICS OF CORONAL LOOP IN DIFFERENT HEATING REGIMES

R. Susino[1], A. C. Lanzafame[1,2], A. F. Lanza[2], D. Spadaro[2]

[1]Dipartimento di Fisica e Astronomia - Sezione Astrofisica, Università di Catania, via S. Sofia 78, I-95123 Catania, Italy
[2]INAF-Osservatorio Astrofisico di Catania, via S. Sofia 78, I-95123 Catania, Italy

INTRODUCTION

Solving the problem of the heating of the solar corona is presently one of the major issues in solar physics. In particular, the question whether the plasma heating inside coronal loops is the effect of steady or impulsive processes, uniform or localized within the structure, is still open.

While the first models of loop heating (e.g., Rosner et al. 1978; Serio et al. 1981), considering magnetic flux tubes in hydrostatic equilibrium under the effects of steady uniform heating, allow to reproduce quite satisfactorily a large number of characteristics in the X-ray and EUV coronal emission of the Sun, recent TRACE and SOHO observations have provided evidence that a large majority of coronal loops, although appearing in quasi-static conditions, cannot be described by loop models in hydrostatic equilibrium (Porter & Klimchuk 1995, Aschwanden et al. 1999, 2001; Winebarger et al. 2003; Patsourakos et al. 2004).

These discrepancies could be explained if coronal loops are assumed to consist of unresolved magnetic strands, each of them heated impulsively and non-uniformly, at different times from its neighbors (Cargill 1994; Klimchuk & Cargill 2001; Spadaro et al. 2003; Cargill & Klimchuk 2004; Reale et al. 2005; Patsourakos & Klimchuk 2005; Klimchuk 2006; Klimchuk et al. 2008).

In this Poster we present results from a set of hydrodynamic simulations of coronal magnetic loop strands undergoing different kinds of heating regimes.

NUMERICAL MODEL AND SIMULATIONS

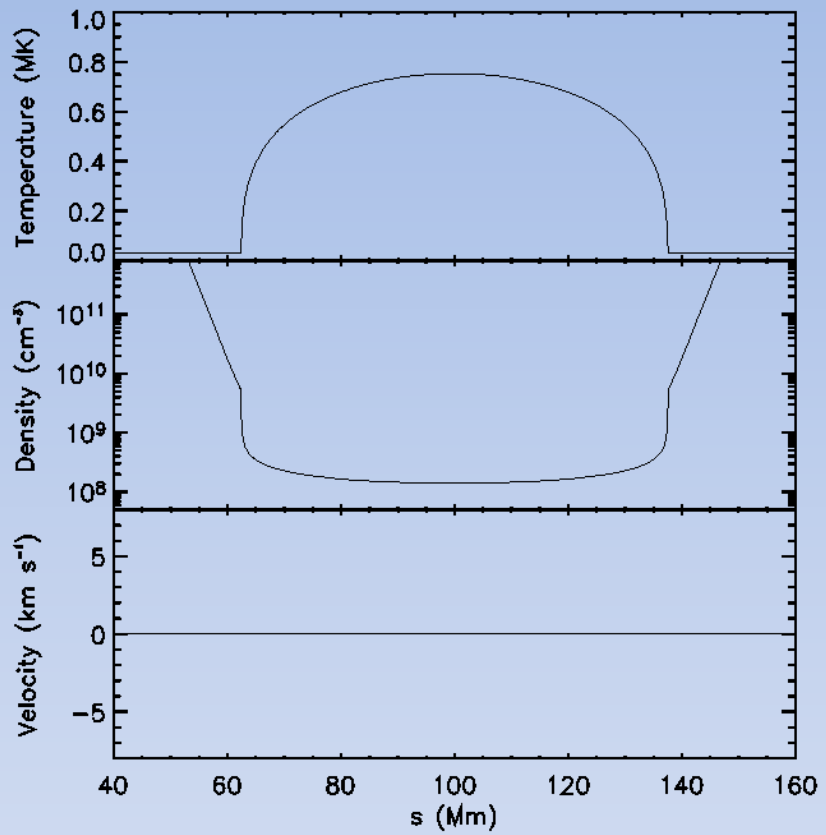

Fig. 1 *Instantaneous profiles of the loop temperature (top panel), density (middle panel), and velocity (bottom panel), vs. the curvilinear coordinate s at the end of the relaxation.*

We simulate a 80 Mm long, active region loop, with initial apex temperature of ~ 0.75 MK. At each footpoint, the loop model is provided with a 60 Mm long, highly dense chromospheric segment, that is maintained at a constant temperature of about 30000 K.

The loop is initially settled into a quasi-static equilibrium state (see Fig. 1), achieved by letting it relax under the action of a steady, uniform background heating.

We subsequently inject into the coronal segment of the loop a swarm of energy pulses (nanoflares) with constant cadence, duration, and amplitude.

We contrast two different heating spatial distributions: uniform vs. localized near the loop footpoints, with an asymmetry between its legs. The heating rate applied in the chromosphere is maintained uniform and steady (see Fig. 2).

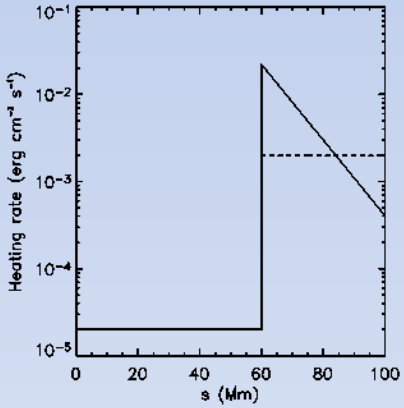

Fig. 2 *Heating rate function vs. the curvilinear coordinate s along half of the loop model, for the localized (solid line) and uniform (dashed line) regimes.*

The cadence time between the energy pulses, t_C, is fixed taking into account the characteristic radiative cooling time of the loop, τ_{cool}, that in our case results ~ 1000 s. The amount of energy released by each nanoflare, E_P, ranges from 0.5×10^{24} erg to 4.0×10^{24} erg.

PLASMA DYNAMICS

In the uniform heating regime the model settles into a new quasi-static equilibrium state (see Fig. 3). The time-averaged apex temperature and density for this new state are consistent with the hydrostatic scaling laws defined by Rosner et al. (1978). Conversely, asymmetric localized heating causes long-term fluctuations due to cycles of plasma condensation formation, motion along the loop, and falling onto the nearest and less heated footpoint.

The condensation is the effect of the occurrence of a thermal instability near the loop top, where the energy supply is not sufficient to balance the radiative losses induced therein by the increase of the density due to the strong chromospheric evaporation. This leads to a progressive cooling of the material located close to the loop apex, and to the formation of a condensation (see Fig. 4).

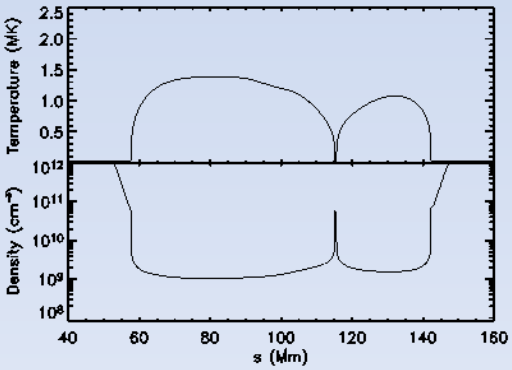

Fig. 4 *Instantaneous profiles of the loop temperature (upper panel) and density (lower panel) vs. the curvilinear coordinate s, for the run whose evolution is shown in Fig. 3, at 2.7 hours after the start of the additional heating. The chromospheric segments have been truncated to highlight the coronal part of the loop.*

Fig. 3 *Initial part of the temporal evolution of the model temperature (top panels), density (middle panels), and velocity (bottom panels), averaged over the upper ¾ of the loop coronal segment, for uniform (left panels) and localized (right panels) heating. In both cases, $E_P = 10^{24}$ erg and $t_C \sim ¼\ \tau_{cool}$. The vertical dashed lines in the right panels approximatively mark the maximum of the condensation phase, whose snapshot is given in Fig. 4.*

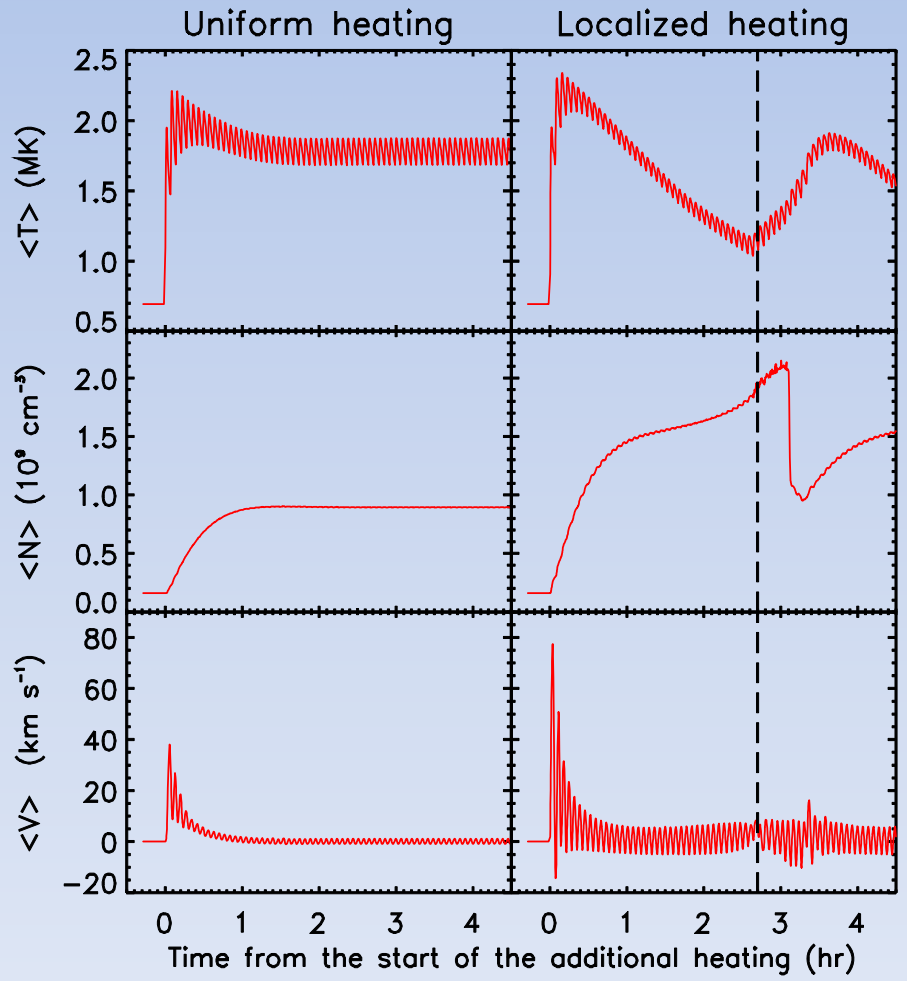

Variation of the nanoflare cadence time

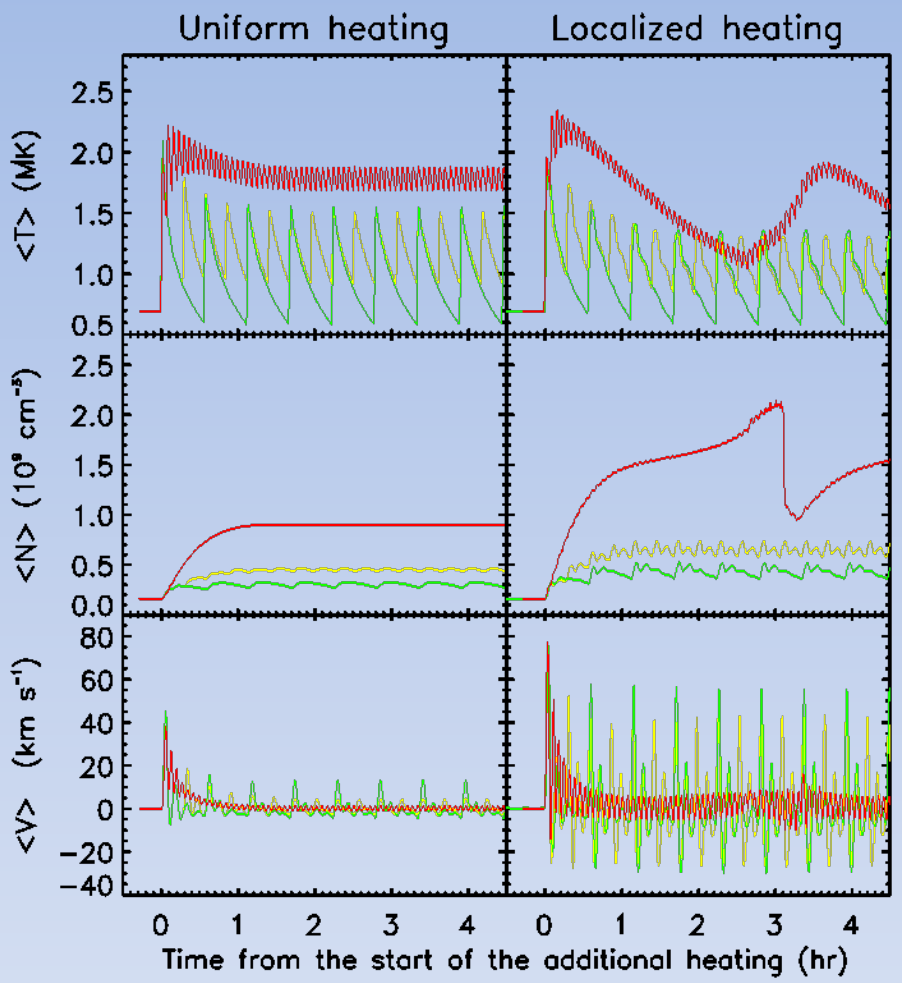

Fig. 5 *As in Fig. 3, for the runs characterized by different nanoflare cadence times, in the uniform (right panels) and localized (left panels) heating regimes: $t_C \sim ¼\ \tau_{cool}$ (red lines), $t_C \sim \tau_{cool}$ (yellow lines), and $t_C \sim 2\ \tau_{cool}$ (green lines). In all cases $E_P = 10^{24}$ erg.*

Plasma condensation does not form when the pulse cadence time is comparable to (t_C = 1000 s) or exceeds (t_C = 2000 s) the radiative cooling time τ_{cool} (see Fig. 5), both with uniform and localized heating. In these cases the long time interval between consecutive pulses allows the system to cool down to nearly the initial temperature, thus preventing the onset of a thermal instability.

Localized heating leads to a more dynamic evolution of the loop model than uniform heating (as it is evident from the velocity temporal profiles), owing to the higher heating rates resulting in the localized heating regime.

Variation of the nanoflare energy amplitude

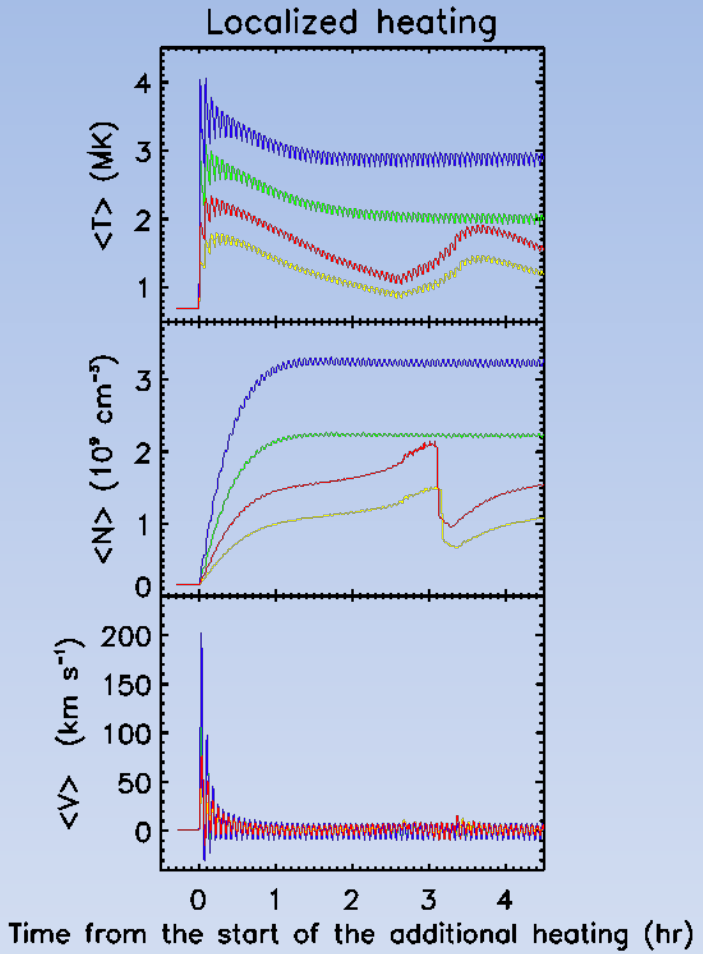

Fig. 6 *As in Fig. 3, for the runs characterized by different values of the nanoflare energy: E_P = 0.5 × 10^{24} erg (yellow line), E_P = 10^{24} erg (red line), E_P = 2.0 × 10^{24} erg (blue line), E_P = 4.0 × 10^{24} erg (green line). In all cases $t_C \sim ¼\ \tau_{cool}$.*

The increase of the pulse energy to 2.0 × 10^{24} erg or 4.0 × 10^{24} erg (see Fig. 6) inhibits the occurrence of the thermal instability and the formation of plasma condensations, probably because the energy supply to the loop center is, in these cases, sufficient to balance the radiative losses and conductive flux therein, even in the presence of localized heating, due to the enhanced energy deposition at the loop footpoints.

When E_P = 0.5 × 10^{24} erg the loop evolves qualitatively in the same way as the case with E_P = 10^{24} erg.

DIFFERENTIAL EMISSION MEASURE

Comparison of our modeling with observations is done using the differential emission measure, DEM(*T*) (e.g., Craig & Brown 1976), which effectively describes the plasma distribution in temperature.

We simulate the observation of a multi-stranded loop computing a single DEM curve by averaging instantaneous DEMs calculated at n = 300 different times, randomly selected throughout each simulation.

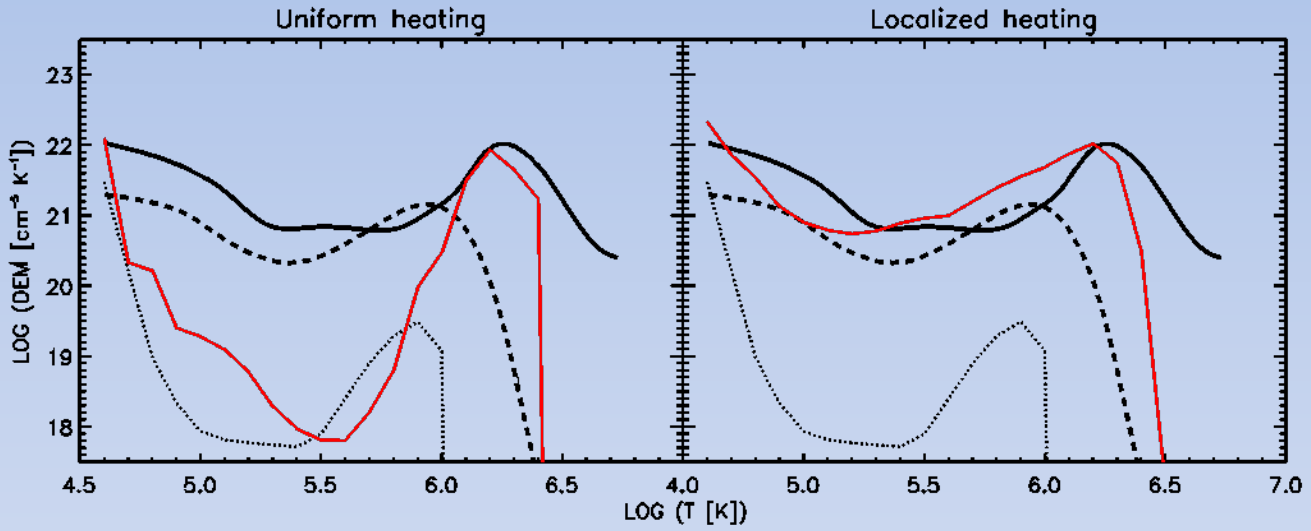

Fig. 7 *Time-averaged differential emission measure (DEM) computed for uniform (left panel) and localized (right panel) heating. In both cases, $E_P = 10^{24}$ erg and $t_C \sim ¼\ \tau_{cool}$. Also reported are the DEMs obtained from SERTS-89 data, relative to an observed solar active region (black solid thick line), and that computed from SOHO-CDS data, pertaining to the quiet Sun (black dashed thick line). The dotted black line is the DEM obtained from our simulations at the end of the relaxation phase, corresponding to Rosner et al. (1978) model with an apex temperature of 0.75 MK.*

As it appears evident, in the localized heating regime the occurrence of condensation formation cycles determines a significant contribution to the transition region temperature part of the DEM (see Fig. 7), owing to the high density and low temperature plasma filling the condensation itself, while the absence of condensations in the uniform heating case leads to a much smaller contribution in the same temperature interval.

The DEM computed for the locally heated loop nicely reproduces the general features of the observed DEM profiles. Conversely, the DEM computed for the uniform heating case may fit conditions in which quasi-isothermal coronal structures are observed (e.g., Schmelz et al. 2009).

Variation of the nanoflare cadence time

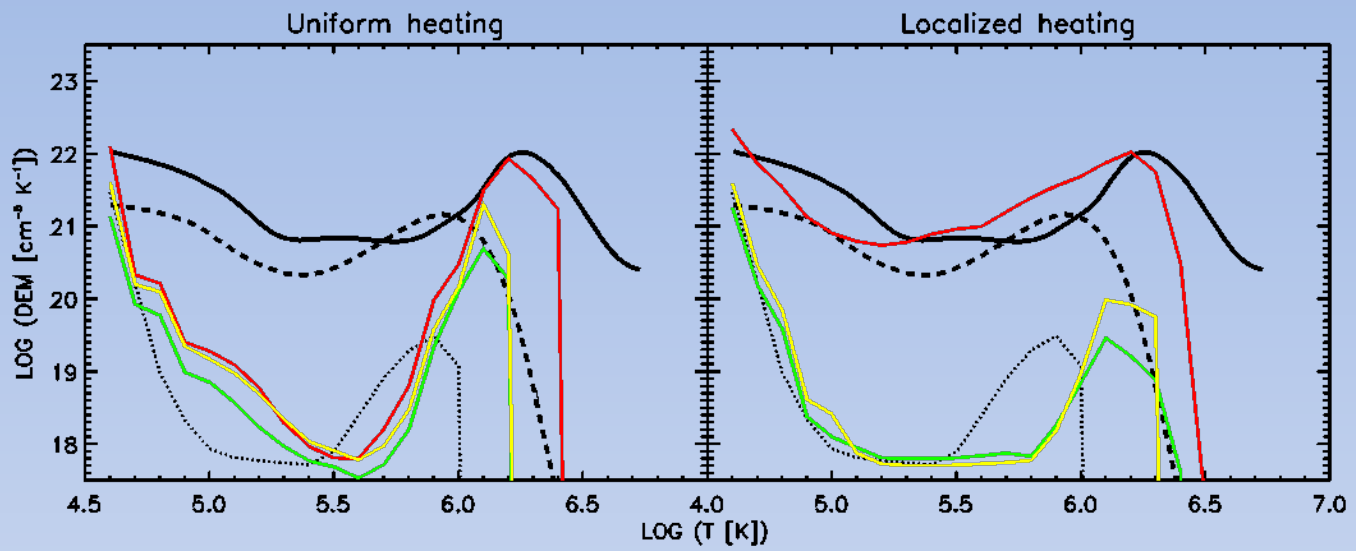

Fig. 8 *As in Fig. 7, for the runs characterized by different nanoflare cadence times, in the uniform (right panel) and localized (left panel) heating regimes: $t_C \sim ¼\ \tau_{cool}$ (red lines), $t_C \sim \tau_{cool}$ (yellow lines), and $t_C \sim 2\ \tau_{cool}$ (green lines). In all cases $E_P = 10^{24}$ erg.*

Simulations with cadence times comparable to, or longer than the radiative cooling time produce DEMs very similar to the case $t_C < \tau_{cool}$ with no condensation (see Fig. 8). The ratio between the maximum and minimum values of the observed DEMs could be anyway reproduced, at least in the localized heating regime, but densities, and therefore DEMs, are in any case well lower than the observed ones.

Variation of the nanoflare energy amplitude

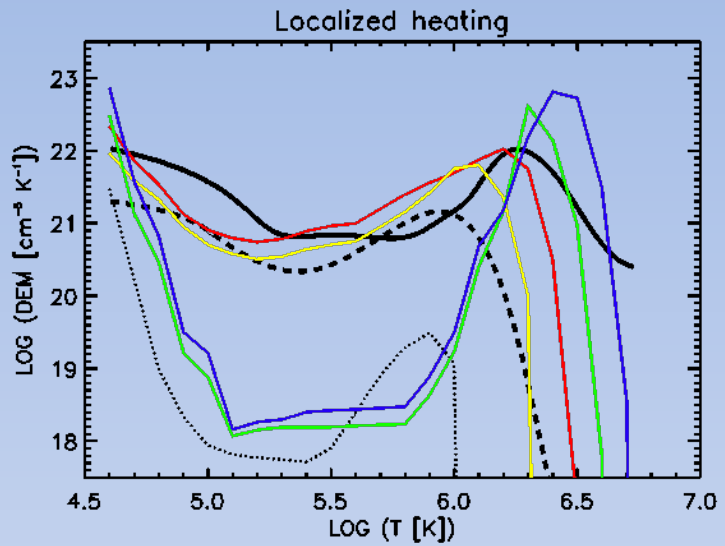

Fig. 9 *As in Fig. 7, for the simulations characterized by different values of the nanoflare energy: E_P = 0.5 × 10^{24} erg (yellow line), E_P = 10^{24} erg (red line), E_P = 2.0 × 10^{24} erg (green line), E_P = 4.0 × 10^{24} erg (blue line). In all cases $t_C \sim ¼\ \tau_{cool}$.*

The DEM computed for the localized heating case with E_P = 0.5 × 10^{24} erg (see Fig. 9) better resembles the observed quiet Sun DEM, at least at transition region temperatures ($5.0 \leq \log T \leq 5.8$), while at coronal temperatures ($\log T > 6.0$) the differences are more pronounced.

The increase of the nanoflare energy over 2.0 × 10^{24} erg causes, as expected, a systematic shift of the DEM maximum toward higher temperatures and the enhancement of the DEM values at coronal temperatures, but the absence of condensation formation in these high-energy regimes determines a lack of contribution at transition region temperatures, so in this temperature interval the curves show the same deep minimum as in the case of uniform heating.

CONCLUSIONS

Hydrodynamic models of coronal loop strands show that the plasma distribution in temperature in the transition region is mostly determined by condensations arising from localized heating at loop footpoints.

Conversely, quasi-isothermal structures at coronal temperature are predicted in the absence of condensations, i.e. when the heating occurs more uniformly along the loop or when the details of the energy deposition (such as the pulse cadence, the pulse energy, or the heating damping-length contrasted to the radiative cooling time or the loop length) prevent plasma condensation.

REFERENCES

Aschwanden, M. J., Newmark, J. S., Delaboudinière, J.-P., Neupart, W. M., Klimchuk, J. A., Gary, G. A. et al. 1999, ApJ, 515, 842

Aschwanden, M., Schrijver, C. J., & Alexander, D. 2001, ApJ, 550, 1036

Cargill, P. J. 1994, ApJ, 422, 381

Cargill, P. J. & Klimchuk, J. A. 2004, ApJ, 605, 911

Craig, I. J. D. & Brown, J. C. 1976, A&A, 49, 239

Klimchuk, J. A. 2006, Sol. Phys., 234, 41

Klimchuk, J. A., Patsourakos, S., & Cargill, P. J. 2008, ApJ, 682, 1351

Klimchuk, J. A. & Cargill, P. J. 2001, ApJ, 553, 440

Lanzafame, A. C., Brooks, D. H., Lang, J., Summers, H. P., Thomas, R. J., & Thompson, A. M. 2002, A&A, 384, 242

Lanzafame, A. C., Brooks, D. H., and Lang, J. 2005, A&A, 432, 1063

Patsourakos, S., Klimchuk, J. A., & MacNeice, P. J. 2004, ApJ, 603, 322

Patsourakos, S. & Klimchuk, J. A. 2005, ApJ, 628, 1023

Porter, L. J. & Klimchuk, J. A. 1995, ApJ, 454, 499

Rosner, R., Tucker, W. H., & Vaiana, G. S. 1978, ApJ, 220, 643

Schmelz, J. T., Nasraoui, K., Rightmire, L. A., Kimble, J. A., Del Zanna, G., Cirtain, J. W., DeLuca, E. E., and Mason, H. E. 2009, ApJ, 691, 503

Serio, S., Peres, G., Vaiana, G. S., Golub, L., & Rosner, R. 1981, ApJ, 243, 288

Spadaro, D., Lanza, A. F., Lanzafame, A. C., Karpen, J. T., Antiochos, S. K., Klimchuk, J. A., & MacNeice, P. J. 2003, ApJ, 582, 486

Winebarger, A. R., Warren, H. P., & Mariska, J. T. 2003, ApJ, 587, 439

Contact: *sur@oact.inaf.it*